Pergamon

PII: S0022-3697(97)00208-4

J. Phys. Chem Solids Vol 59, No. 3, pp. 435–445, 1998

Printed in Great Britain
0022-3697/98 $19.00 + 0.00

LITHIUM OXIDE AND SUPERIONIC BEHAVIOUR—A STUDY USING POTENTIALS FROM PERIODIC AB INITIO CALCULATIONS

R. M. FRACCHIA†[a], G. D. BARRERA†[a], N. L. ALLAN[a], T. H. K. BARRON[a] and W. C. MACKRODT[b]

[a]School of Chemistry, University of Bristol, Cantock's Close, Bristol BS8 1TS, UK
[b]School of Chemistry, University of St. Andrews, St. Andrews, Fife KY16 9ST, UK

(*Accepted* 7 *January* 1997)

Abstract—A simple general methodology for obtaining interionic potentials from periodic ab initio calculations is presented, using periodic Hartree–Fock theory as implemented in the program CRYSTAL. To test the approach, two-body potentials are generated for Li_2O. Results obtained from our new potential are compared with those from previously suggested empirical potentials, paying most attention to the possibility of superionic behaviour in this material at high temperatures. The application of ab initio Hartree–Fock theory, lattice statics, lattice dynamics and molecular dynamics is able to provide a consistent picture of a superionic transition in lithium oxide at 1100 K. Details of the mechanism of the transition are discussed with the aid of the calculated dispersion curves at high temperature, and individual molecular dynamics trajectories. © 1997 Elsevier Science Ltd. All rights reserved.

Keywords: C. ab initio calculations, D. anharmonicity, D. lattice dynamics, D. phonons, D. phase transitions

1. INTRODUCTION

Many theoretical techniques exist for the study of the solid state, ranging from simulation (lattice statics, lattice dynamics, molecular dynamics) to ab initio methods. Applications of atomistic simulation techniques are limited by the lack of suitable high-quality interatomic potentials, on which the success of any classical simulation depends. Consequently, in recent years increases in computational power together with methodological advances have led to the use of periodic ab initio methods (both density functional [1] and Hartree–Fock techniques [2, 3]) for the determination of ground-state properties of an increasingly wide range of materials [4]. Although temperature effects can, in principle, be calculated from ab initio calculations, the high computational requirements of such work makes this currently unfeasible, and, as in this paper, it is necessary to resort to classical simulation techniques.

Accordingly, in this paper we show how to extract suitable potentials for classical simulations by calculating them directly using periodic ab initio Hartree–Fock techniques. No empirical data is used in our procedure and the proposed methodology is quite general. Although it is often tempting in simulation studies to use empirical potentials fitted to experimental data, some doubts must remain as to the reliability of such potentials for conditions significantly different from those for which experimental data are available. It is especially important to have confidence in the potentials for simulations of defects (particularly interstitials).

The traditional approach to the calculation of non-empirical potentials is the electron-gas model [5]. Such electron-gas potentials have been widely used [5], and appear to be more successful than would be expected from the crude approximations of the model. Unlike the electron-gas model, which calculates the interaction energy between two ions with integral charge, the method suggested here makes no assumption as regards ionicity. Our scheme also differs from that used by Gale et al. [6], who use periodic ab initio Hartree–Fock calculations to obtain potentials for static properties of α-Al_2O_3, in that no multiple fitting of potentials to a hypersurface is involved.

Unlike most previous work, we test our potentials by calculating thermal properties. We have chosen to study lithium oxide (Li_2O), which is not only of considerable technological interest as a lithium ion conductor ('solid electrolyte') [7] but is also a possible blanket material for fusion reactors [8]. The relative simplicity of its crystal structure (antifluorite as shown in Fig. 1) has led to its being the subject of both considerable experimental [9–13] and theoretical study [14–18], much of which has been concerned with fundamental aspects of ion transport and the possibility of 'superionic' behaviour. Because of experimental difficulties with Li_2O at high temperature, this transition, strongly suggested by neutron scattering results [13], has not been fully established from conductivity or NMR studies [12].

† Permanent address: Universidad de Buenos Aires, Facultad de Ciencias Exactas y Naturales, Departamento de Química Inorgánica, Analítica y Química Física, Pabellón 2, Ciudad Universitaria, 1428 Buenos Aires, Argentina.

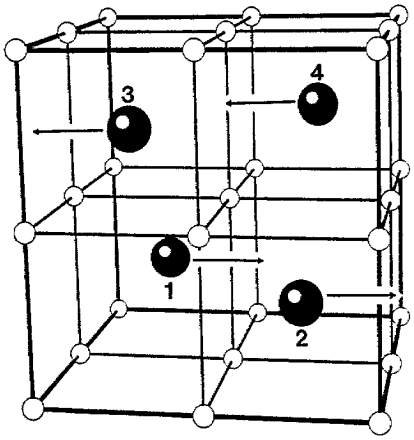

Fig. 1. The antifluorite crystal structure of Li_2O. The conventional cubic cell is shown with the oxygen atoms numbered for reference.

2. DERIVATION OF POTENTIALS

All our simulations use potentials obtained from the results of periodic Hartree–Fock calculations, as implemented in the CRYSTAL 92 code [3]. We have taken the basis set from a previous Hartree–Fock study of Li_2O [19], but have added a single *d*-function to both cations and anions. The important rôle of *d*-functions in the calculation of phonon frequencies for oxides (which involves the displacement of sets of ions from their equilibrium positions, the concern also of the present paper) has been stressed by McCarthy and Harrison [20]. The exponents of these functions were optimised at a lattice parameter of 4.573 Å (the calculated value of the lattice parameter a_0 in Ref. [19]). At the same time, the outer sp functions on the cation and anion were reoptimised. The changes to the basis set published in Ref. [19] are listed in Table 1. The calculated equilibrium lattice parameter using the new basis is 4.568 Å.

In their study of α-Al_2O_3 [6], Gale et al. employed 38 configurations to fit simultaneously all the required Buckingham potential parameters. This is a somewhat cumbersome procedure and so we have adopted a more direct strategy. As in most classical simulations, it is assumed that the energy of the crystal can be written as a sum of pairwise interactions. For the Coulombic part, the calculated Mulliken charges for Li and O are used ($0.944e$ and $-1.888e$ respectively). For simplicity the Li–Li interaction is assumed to be purely Coulombic. For the non-Coulombic contribution, the energy for each pairwise interaction is fitted separately. To generate the Li–O potential we first calculate the variation in energy as a function of the relative displacements of the oxygen and lithium sublattices, as shown in Fig. 2. Since the lithium–lithium and oxygen–oxygen distances are unaffected by this displacement, this should give information directly about the Li–O interaction. Displacements in the [1,0,0], [1,1,0] and [1,1,1] directions were considered with successive steps of $(\delta,0,0)$, $(\delta,\delta,0)$, (δ,δ,δ) in each direction and δ increased from 0 to 0.4 Å in steps of 0.05 Å. For simplicity we have chosen to fit these results to a Buckingham potential, of the form

$$V(r) = A\exp(-r/\rho) - C/r^6$$

where A, ρ and C are constants, with a cutoff of 12 Å. All three curves in Fig. 2 were fitted simultaneously, giving the Li^+–O^{2-} potential parameters tabulated in Table 2. The distortion energies given by these potentials agree with the Hartree–Fock values to better than 1% in all three directions.

For the oxygen–oxygen potential, we displace the oxygen atoms labelled in Fig. 1. We displace oxygens 1 and 2 by δ in the [1,0,0] direction and oxygens 3 and 4 by δ in the $[-1,0,0]$ direction. Values of δ from 0 to 0.4 Å were taken in steps of 0.05 Å. The energy vs. distortion curve is shown in Fig. 3. Under this displacement both Li–O and O–O distances alter. We determine the change in energy due to the change in the Li–O distances using the previously fitted Li–O potential. From this it is straightforward to obtain the change in energy due to the variation of the O–O distance. A Buckingham potential is then fitted (Table 2). Fig. 3 shows the energy vs. distortion curve for the final set of potentials; again the difference between the Hartree–Fock and fitted-potential value is less than 1% at all points.

At this point it is instructive to compare our fitted potentials with some other recent sets in the literature. Figs 4 and 5 show the non-Coulombic contributions to other Li–O and O–O potentials proposed recently [14, 21–23]. The potentials used in Ref. [21] have not been tabulated previously and so are also listed in Table 2. All these other potentials, unlike the one we have derived from the Hartree–Fock calculations, assume complete ionicity. Three of the sets of potentials (from Refs. [14, 21, 22]) were obtained by empirical fitting. The potentials obtained here are also shown together with a further potential derived recently using the modern valence bond formalism discussed in Ref. [23]. The starting point for the calculation of this last potential was to take wavefunctions for Li^+ and O^{2-} ions embedded in a simulated Madelung potential. It is worth noting that the empirical potentials were generally obtained by fitting procedures considering only the static contribution to properties, neglecting vibrational contributions completely. It is also important to appreciate the limitations

Table 1. New outer shell basis set exponents used in the present work. These were used to supplement the basis in Ref. [19]

Oxygen ion		Lithium ion	
4sp	0.1421	2sp	0.5278
3d	0.6419	3d	0.5312

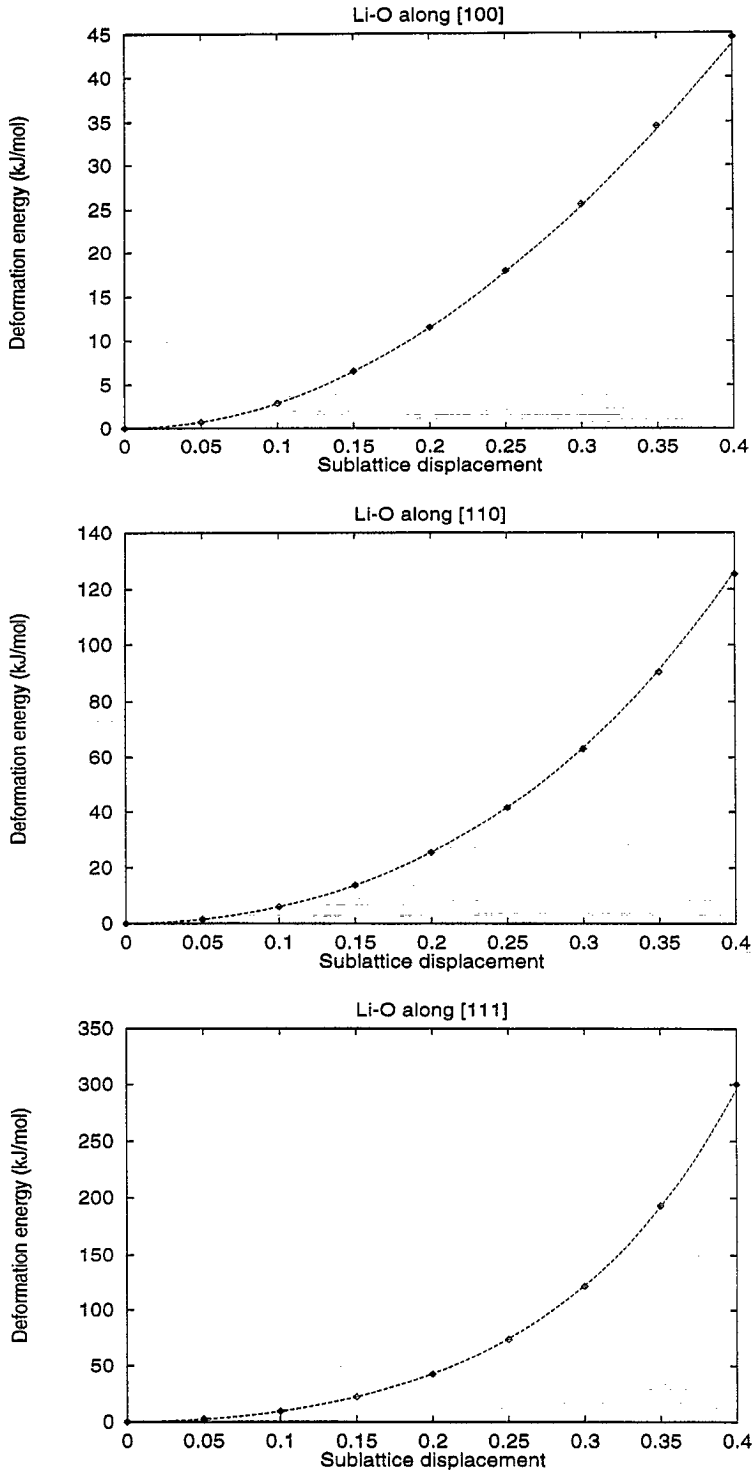

Fig. 2. Energy (kJ mol^{-1}) vs. displacement δ (Å) for relative displacements of the oxygen and lithium sublattices. Displacements in the [1,0,0], [1,1,0] and [1,1,1] directions were considered with successive steps of (δ,0,0), (δ,δ,0), (δ,δ,δ) in each direction with δ increased from 0 to 0.4 Å in steps of 0.05 Å. These points are marked ◇. For comparison, the dotted lines are the curves predicted by the final fitted Li–O potential.

in the Hartree–Fock calculations in that correlation (including dispersion) is not included.

In comparing the different potentials it is important to bear in mind both the range of interionic distances sampled in the Hartree–Fock calculations, and the separations likely to be important in the calculations using these potentials, indicated in the legends of Figs 4 and 5. Our potentials are only likely to be reliable over the ranges of internuclear separation sampled in the procedure used in potential generation. For studying the

Table 2. Potential parameter sets for Li_2O. For each pairwise interaction $V(r) = A\exp(-r/\rho) - C/r^6$, with a cutoff of 12 Å. Further discussion is given in the text

Interaction	A (eV)	ρ (Å)	C (eV Å^6)
This work			
Li^+/Li^+	0.0	1.0	0.0
Li^+/O^{2-}	653.84	0.285723	0.0
O^{2-}/O^{2-}	0.0	1.0	−76.651
Allan et al. [21]			
Li^+/Li^+	0.0	1.0	0.0
Li^+/O^{2-}	525.95	0.3010	0.0
O^{2-}/O^{2-}	22764.3	0.1490	20.37

Where the shell model was used in lattice dynamics calculations with these potentials, the oxygen shell charge was $-2.9769e$ and the spring constant 47.6908 eV Å^{-2}.

thermal expansion and the superionic transition the Li–O potential is likely to be the most important.

There are clearly large differences between the various potentials, particularly at the nearest neighbour Li–O (≈ 2.3 Å) and O–O distances (≈ 3.3 Å). In particular, the potentials due to Bush et al. [22] differ considerably from all the others. For example at the nearest-neighbour distance, the Bush et al. Li–O potential is much less repulsive than all the others and only the Bush et al. O–O potential is positive at all likely O–O separations. The O–O potential derived from the Hartree–Fock results is negative at the separations sampled, even though dispersion is not included. Some evidence that this is not unreasonable comes from direct calculations of the O–O interionic potential using valence bond theory in Ref. [23].

We now test our derived potential using two types of simulation: lattice statics/dynamics calculations and molecular dynamics.

3. SIMULATIONS

3.1. *Lattice statics and quasiharmonic lattice dynamics*

We work with the Helmholtz free energy of the crystal, A, which, it is assumed, can be written as the sum of static and vibrational contributions,

$$A = \phi_{stat} + A_{vib} \tag{1}$$

The calculation of the vibrational contribution requires the evaluation of the normal mode frequencies $\nu_j(\boldsymbol{q})$, for wavevectors $\boldsymbol{q}$, evaluated from the dynamical matrix. In the quasiharmonic approximation the $\nu_j(\boldsymbol{q})$ are harmonic and independent of the temperature T, but not of the volume V. A_{vib} is given by

$$A_{vib} = \sum_{q,j} \left\{ \tfrac{1}{2} h\nu_j(\boldsymbol{q}) + kT \ln\left[1 - \exp(-h\nu_j(\boldsymbol{q})/kT)\right] \right\} \tag{2}$$

where k is Boltzmann's constant. We sum over the uniform grid of $\boldsymbol{q}$-vectors known as the Chadi–Cohen special points [24]. Other thermodynamic functions follow from straightforward algebraic manipulation, e.g. the entropy (S_{vib}) is given simply by $-(\partial A/\partial T)_V$. At each temperature the corresponding zero-pressure volume was found by minimisation of the Helmholtz free energy ($p = -(\partial A/\partial V)_T$) by numerical differentiation. Derivatives of A were calculated by considering increments in the lattice parameter of 0.001 Å.

Most of our calculations have been rigid ion, but we have also carried out a small number using the shell model for a better representation of the lattice dynamics (see Table 2). Full details of the treatment of the standard shell model employed can be found in Ref. [25].

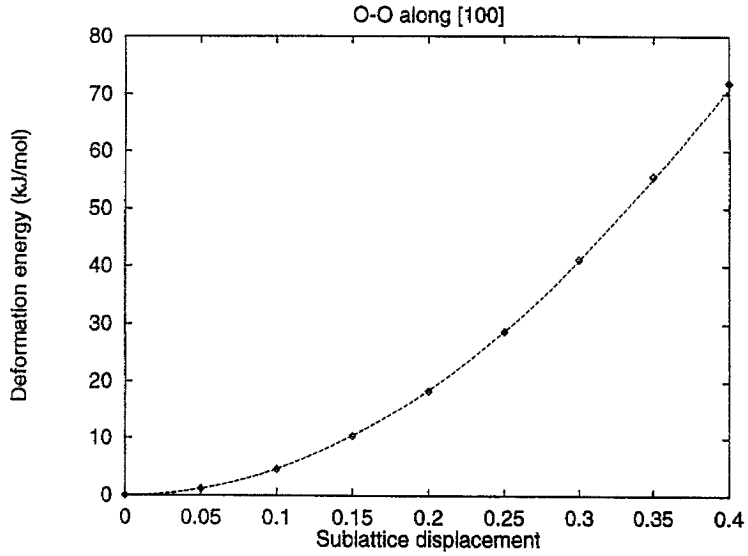

Fig. 3. Energy (kJ mol^{-1}) vs. displacement δ (Å) for relative displacements of the oxygen ions. Referring to the numbering scheme in Fig. 1, oxygens 1 and 2 are displaced by δ in the [1,0,0] direction and oxygens 3 and 4 by δ in the [− 1,0,0] direction. Successive displacements δ from 0 to 0.4 Å in steps of 0.05 Å were considered. These points are marked ◇. For comparison, the dotted lines are the curves predicted by the final fitted set of potentials.

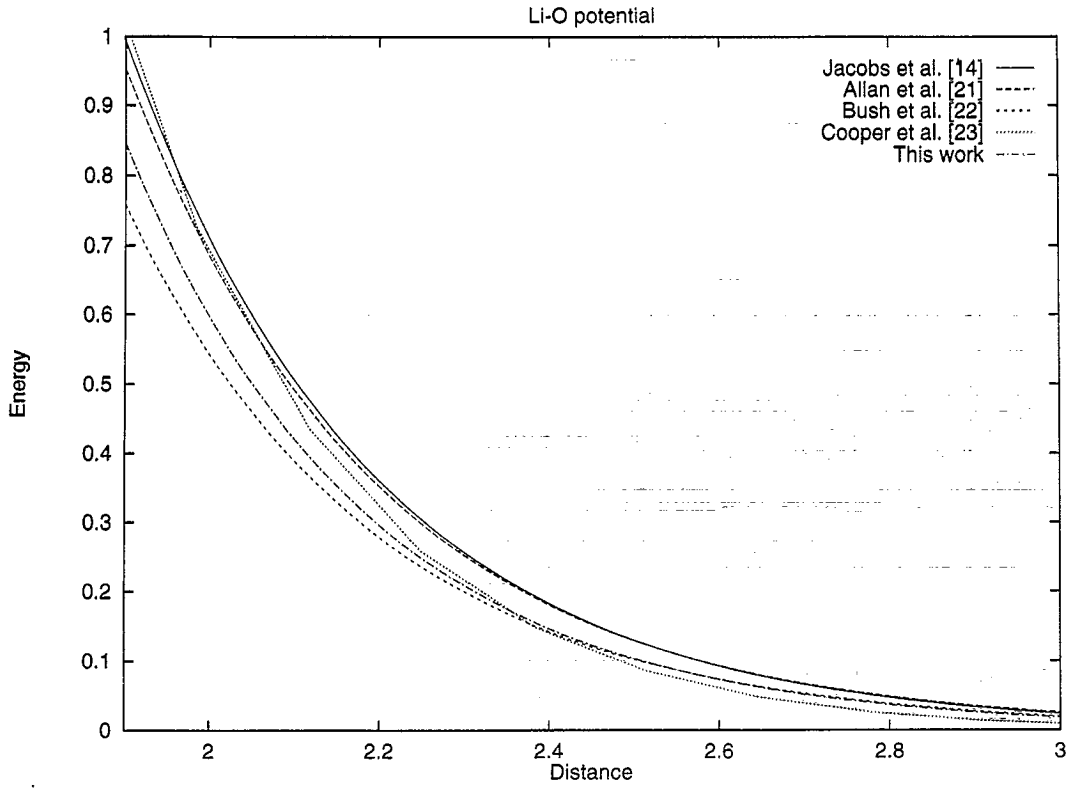

Fig. 4. A comparison of Li–O potentials for Li_2O. The nearest neighbour Li–O distance is $\approx$ 2.3 Å. Energies are in kJ mol^{-1}, distances in Å.

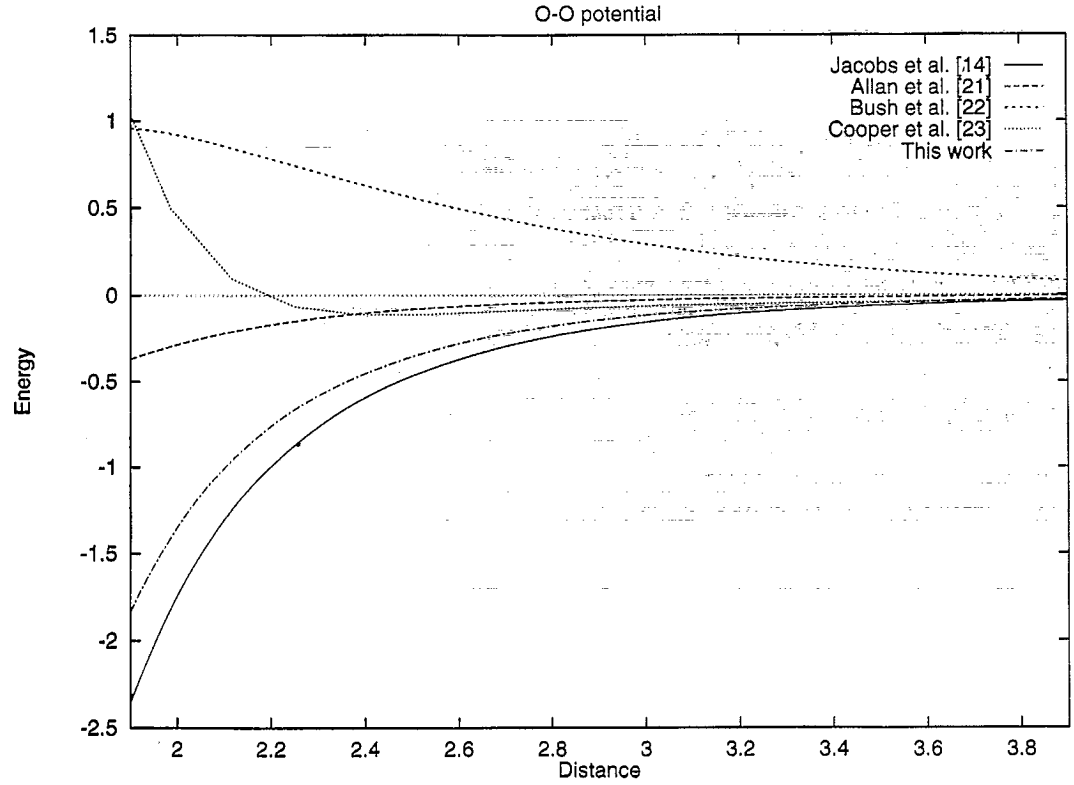

Fig. 5. A comparison of O–O potentials for Li_2O. The shortest O–O distance in the perfect lattice is $\approx$ 3.3 Å. Energies are in kJ mol^{-1}, distances in Å.

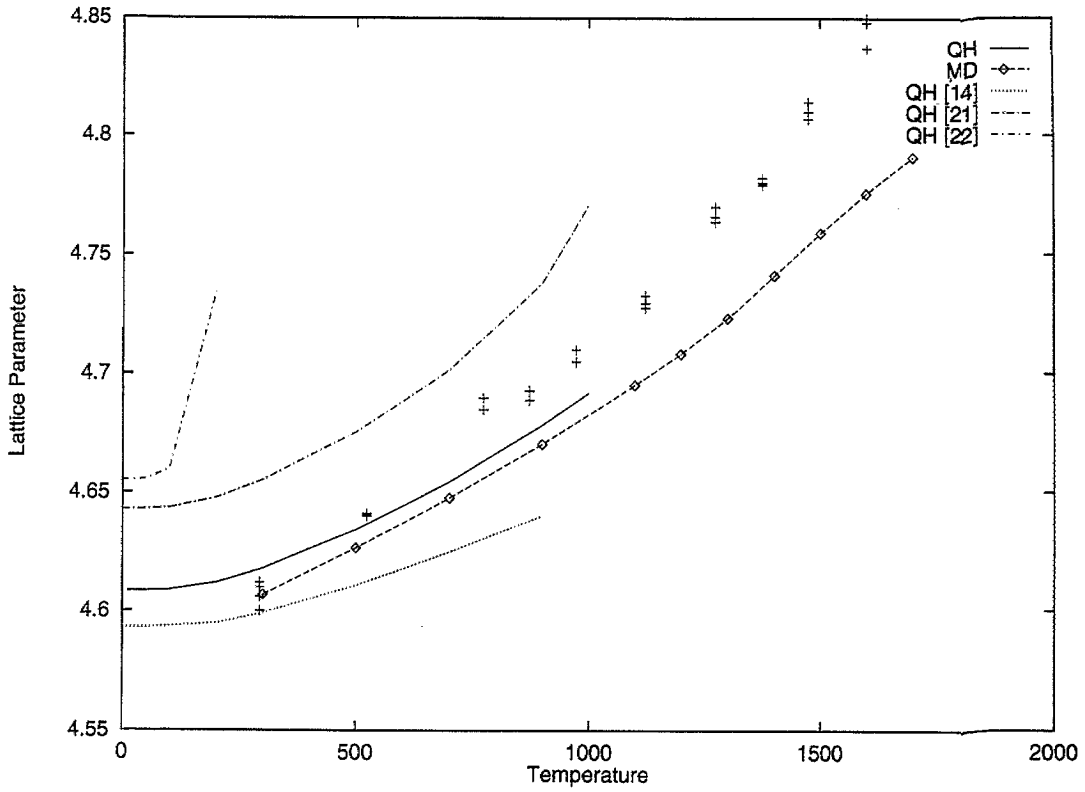

Fig. 6. Calculated and experimental variation of lattice parameter (Å) with temperature (K) for Li_2O. QH denotes results from quasiharmonic lattice dynamics, MD molecular dynamics. Experimental points (+) are taken from Refs. [27, 28, 13].

3.2. *Molecular dynamics*

Here we have used molecular dynamics simulations at constant pressure and temperature with a cell of 768 ions by using an extended system as described, for instance, in Ref. [26]. The same interionic potentials were used as for the lattice dynamics calculations. The initial configuration was generated by arranging 512 Li atoms and 256 O atoms in a cubic box of side length 4×4.60 Å forming the anti-fluorite structure. A constant NVE run of 10 ps was performed to obtain an initial configuration. This configuration was used as the starting point for an equilibration run of 10 ps followed by a production run of 10 ps at constant NPT. The temperature and pressure were kept constant by using an extended system [26] with thermostat and barostat relaxation times of 1 and 0.5 ps respectively. The reliability of the results were checked by considering simulation times longer than 10 ps.

3.3. *Results and discussion*

We start with the thermal expansion of Li_2O. Fig. 6 shows a comparison of the calculated lattice parameter as a function of temperature obtained from quasiharmonic lattice dynamics and molecular dynamics (both rigid ion) using our derived potential. The experimental data are from Kurasawa et al. [27], Hull et al. [28] and Farley et al. [13]. On the scale shown the lattice parameter calculated using shell model quasiharmonic lattice dynamics is indistinguishable from that shown for the rigid ion model (compare the results for MgO in Ref. [29]; at small temperatures the inclusion of the shell-model has little effect; while at higher temperatures it reduces the rate of expansion). It is worth noting that in the same type of calculation the potentials due to Bush et al. [22] fail badly in that imaginary modes appear at temperatures as low as 150 K (Fig. 6). Results from the potentials from Ref. [23] are not shown since they predict larger lattice parameters than all the others considered.

At low temperatures the lattice parameters given by

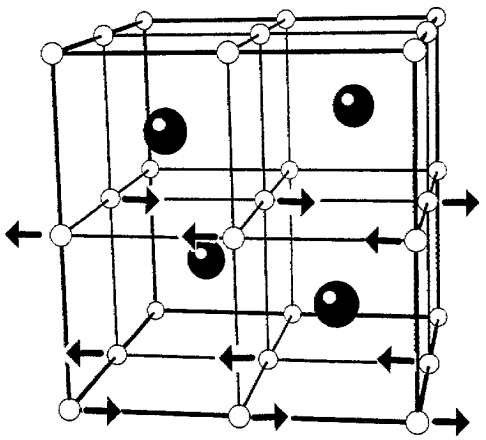

Fig. 7. Soft-mode motion of the Li atoms at $q = (0,0,1)$.

quasiharmonic lattice dynamics are somewhat larger than those given by molecular dynamics, due to the inclusion of zero-point energy in the former but not in the latter. At intermediate temperatures there is closer agreement between the two.

Roberts and White [30] have noted a Schottky-like bump in the temperature variation of the linear thermal expansion coefficient of fluorite crystals (CaF_2, BaF_2, SrF_2, PbF_2, SrF_2) close to the superionic transition (similar to that also observed for the heat capacity, C_p). The experimental data currently available for Li_2O is not sufficiently precise to say whether the same is true of this antifluorite crystal. The MD results do not appear to show such a hump, but the likely accuracy of the simulation is insufficient to establish this. More accurate expansion data at high temperatures are highly desirable.

At higher temperatures the volumes predicted by lattice dynamics (potentials in Table 2) increase very

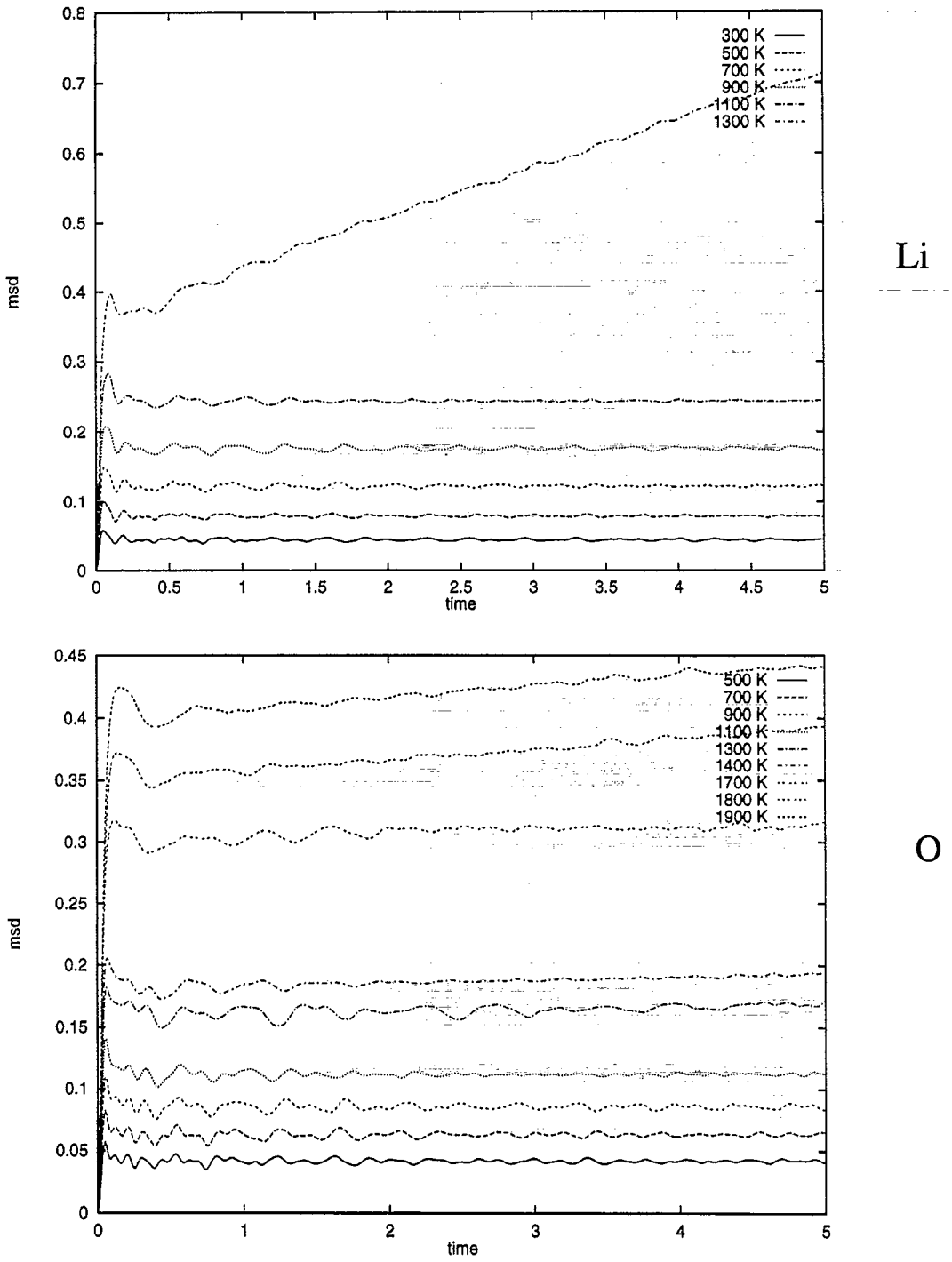

Fig. 8. Time dependent mean square displacements (Å^2) vs. time (ps) for Li and O at a range of temperatures.

rapidly indeed. This non-physical result is due to the appearance of soft modes in the Brillouin zone, as shown by our calculated phonon dispersion curves as a function of temperature. There is a substantial mode softening near (0,0,1) (in units of $2\pi/a$), which has also been noted by Gavartin et al. [17]. This occurs at a temperature close to 1000 K, for both rigid and shell model calculations. Analysis of the eigenvectors indicate this motion involves only motion of the Li sublattices at this point, with lines of Li atoms in the z-direction all moving in the same direction, with atoms in neighbouring lines moving in the opposite direction, as shown in Fig. 7. This is consistent with the observations of Farley et al. [10] that most of the Li motion above the superionic transition occurs via (001 hops). In the lattice dynamics calculations, it is the mode at (0,0,1) which first becomes imaginary; to be followed at higher temperatures by modes at neighbouring q-vectors. It is interesting to note that the highest frequency mode at (0,0,1) also involves motion of the Li sublattices only, with alternate (0,0,1) planes moving in opposite directions.

We now consider the MD results. These show that the system is solid at 1700 K but liquid at 1900 K, in reasonable agreement with the experimental melting point of

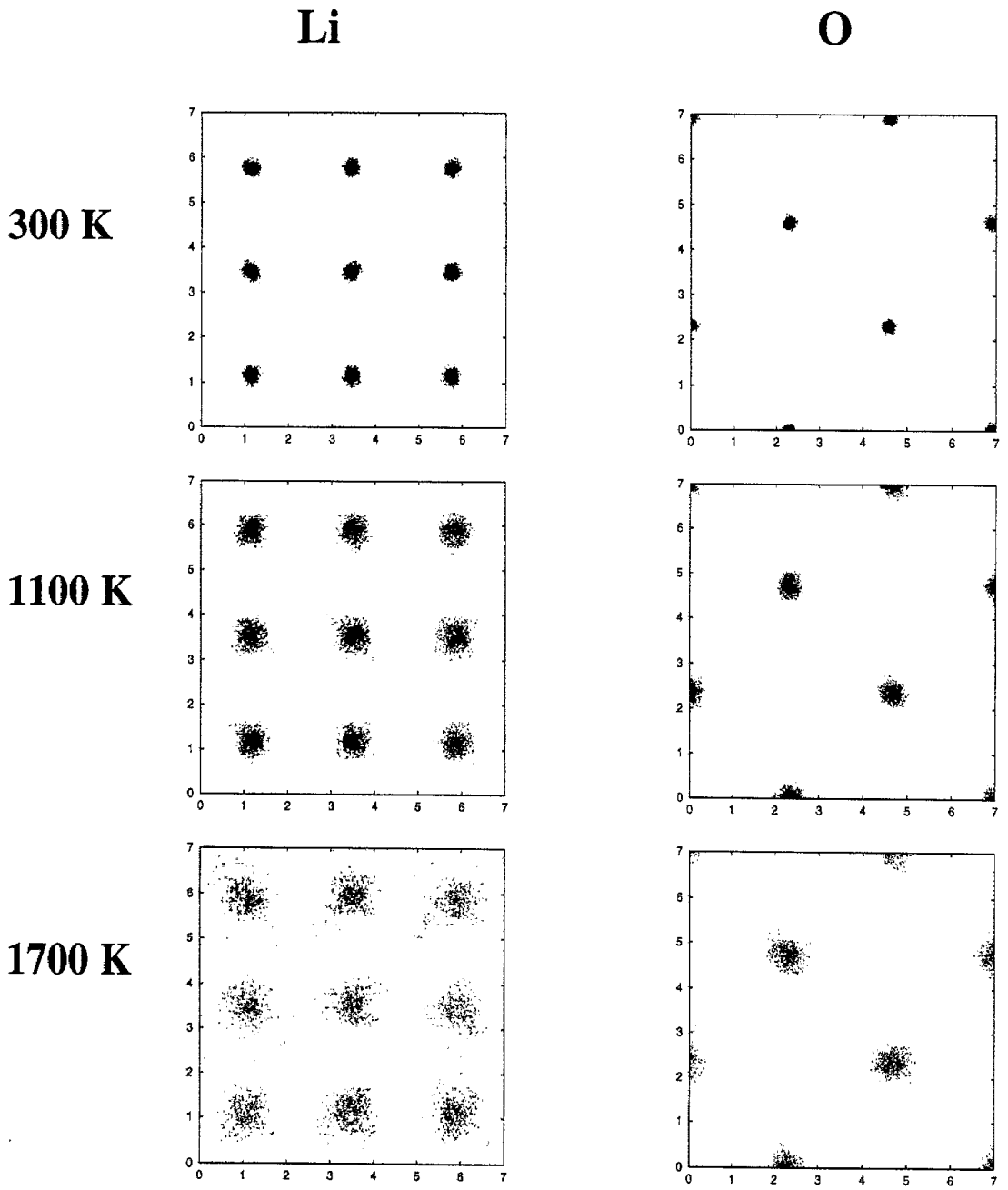

Fig. 9, Trajectories of Li and O ions in Li_2O over 1000 timesteps projected onto the [100] plane at 300 K, 1100 K and 1700 K. Distances marked are in Å.

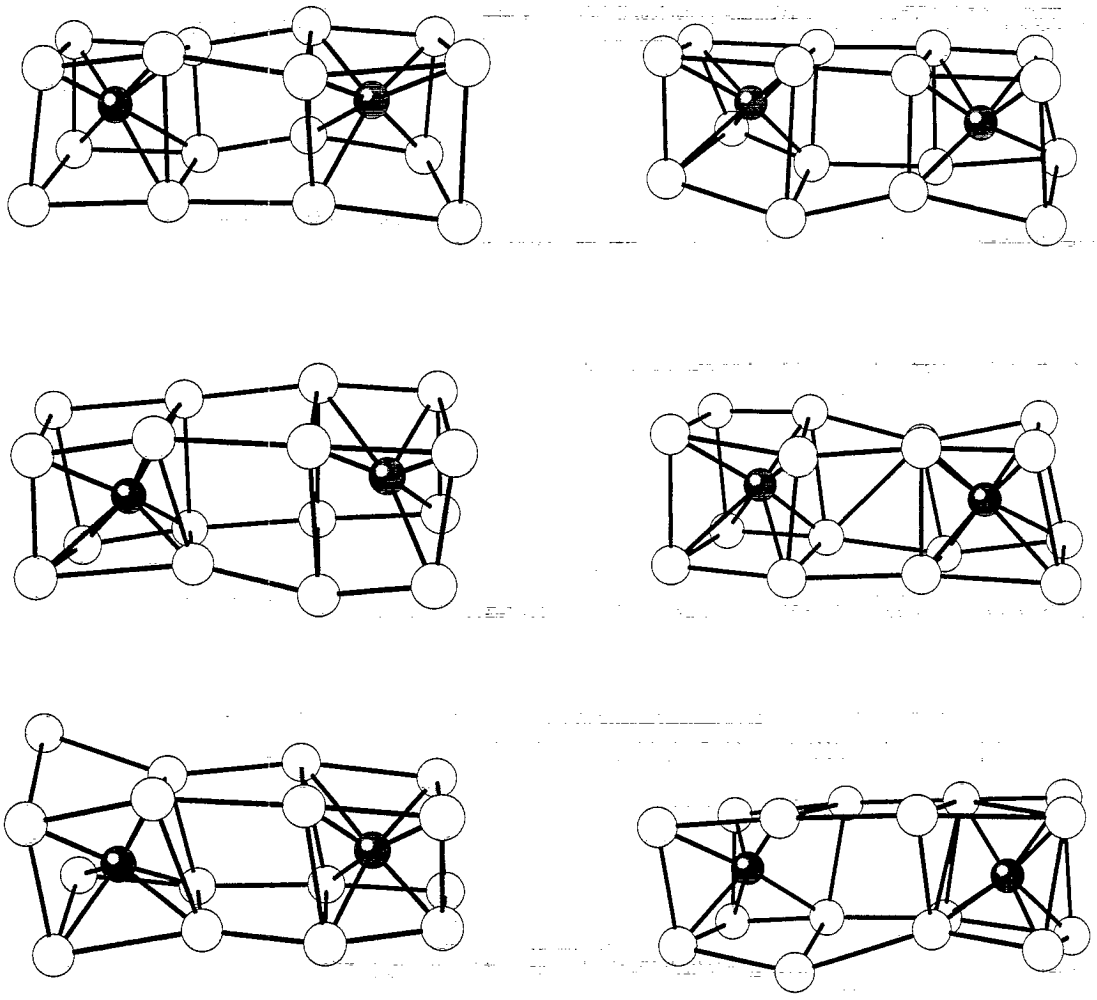

Fig. 10. Part of the Li_2O structure at 900 K and 1100 K. Note the increasing large distortion, as discussed in the text.

1705 K [31]. Fig. 8 shows plots for the time dependent mean square displacement as a function of the time for both cations and anions at a range of temperatures between 300 K and 1300 K. When the temperature is under 1800 K the anion function tends to a constant value at long times, indicating that below this temperature the anions do not diffuse. Above 1100 K, the cation (but not the anion) mean square displacement becomes asymptotically proportional to time, indicating diffusing lithium ions according to the well-known relation,

$$< \Delta r^2 > = B + 6Dt \qquad (3)$$

The onset of lithium diffusion is at a temperature close to that at which we see the imaginary frequency in the lattice dynamics. Just below this temperature the root mean square amplitude of vibration ($\approx$ 0.5 Å) is very large compared to the Li–Li distance ($\approx$ 2.3 Å).

The density plots for Li atoms at 300 K, 1100 K and 1700 K shown in Fig. 9 confirm the large vibrational amplitudes of the Li ions. The behaviour of the O sublattice also shown in this figure is striking in contrast. Such plots for Li over a wider temperature range confirm the conclusions of previous work on fluorite systems that the mobile ions are strongly localised on their regular sites even in the superionic regime close to the melting point, despite their high mobility at such temperatures. Interstitials do not reside at the empty cube centre site in the superionic regime, in agreement with earlier work on fluorites (see, for example, Ref. [32]). Analysis of individual ion trajectories shows that the results do not support a direct interstitial mechanism for the lithium

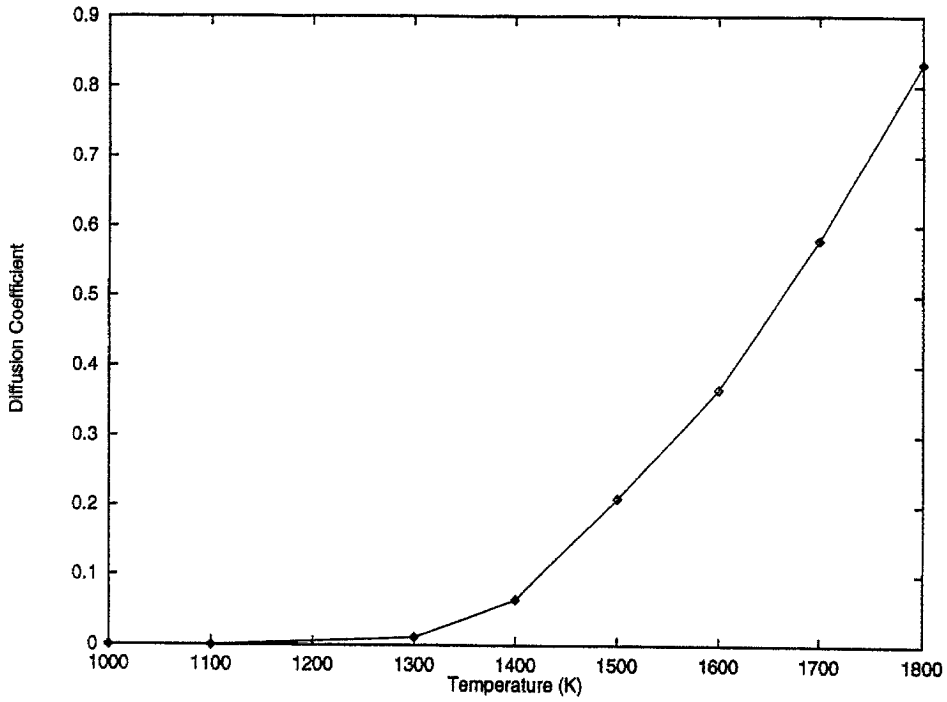

Fig. 11. Calculated Li diffusion coefficients (10^{-4} cm^2 s^{-1}) of Li vs. temperature (K).

motion, again analogously to fluorite systems. Even at relatively low temperatures the unit cell can be considerably distorted consistent with the large root mean square amplitude of vibration for Li, as shown for 900 K in Fig. 10. Close to and above the superionic transition this distortion of the Li sublattice is even greater. For example, Fig. 10 also shows a series of steps at a temperature as low as 1100 K in which one next-nearest-neighbour Li distance can be smaller than a nearest-neighbour Li distance. Overall, the details of the Li diffusion mechanism are considerably more complicated than the simple caterpillar-like interstitial motion along the (0,0,1) direction proposed in Ref. [23].

The calculated diffusion coefficients of Li are shown as a function of temperature in Fig. 11. There is good agreement between experiment and theory. The activation energy for the diffusion process is $\approx$ 1 eV. Oishi and coworkers [33, 34], however, report a value of $\approx$ 2.5 eV for intrinsic Li diffusion and an extrinsic value of $\approx$ 1 eV. Our results suggest that it is the latter value that corresponds to the intrinsic regime, which is also consistent with earlier lattice statics calculations of defect energies [21]. Association between divalent and trivalent impurities and lithium vacancies is a possible explanation for the apparent activation energy of 2.5 eV [21].

4. FINAL REMARKS

In this paper we have presented a simple general methodology for obtaining interionic potentials from periodic ab initio calculations, using here Hartree–Fock theory as implemented in the program CRYSTAL. To test the approach we generated potentials for Li_2O for which empirical potentials were already available and so we were able to compare critically results obtained from our new potential with those from the empirical potentials, paying most attention to the superionic transition in this material. It is clear that the application of ab initio Hartree–Fock theory, lattice statics, lattice dynamics and molecular dynamics is able to provide a consistent picture of the superionic transition in lithium oxide. The mechanism for this is more complex than suggested previously [23]. It is worth pointing out that the results are not highly sensitive to the exact potential cutoff.

Of course, there are approximations inherent in the use of a two-body potential model (e.g. the failure to account for the Cauchy violation in crystals with the rocksalt structure). Our potentials are only likely to be reliable over the ranges of internuclear separation sampled in the procedure used in potential generation. For studying the superionic transition the Li–O potential is likely to be the most important. For situations where the Li–Li distance is likely to be very short then a slightly modified procedure which did not assume a purely Coulombic interaction would be more appropriate. Under large distortions we have found that some charge transfer from O back to Li can take place, which would not be accounted for if this distortion was to be studied using the potentials generated from more symmetric displacements of the atoms. The Hartree–Fock method used here takes no account of correlation. It will be interesting in the

future to apply the methods outlined here for the generation of potentials using ab initio techniques other than Hartree–Fock, such as density functional theory (LDA) [35]; for the properties of non-magnetic insulating oxides important in fitting the potentials the two techniques are roughly comparable.

Our results are sufficiently encouraging for the use of this approach in the future for systems for which there exist insufficient data for the generation of empirical potentials.

Acknowledgements—RMF and GDB gratefully acknowledge financial support from la Universidad de Buenos Aires. GDB's contribution to this work was made possible by means of a grant from el Consejo Nacional de Investigaciones Científicias y Técnicas de la República Argentina, and he also acknowledges the hospitality and advice of M.L. Klein and his group during a visit to the University of Pennsylvania. Computational resources were made available through EPSRC grant GR/K48686 and the Royal Society. This work forms part of a Royal Society/ CONICET Joint Project, which has also funded visits of NLA and THKB to Buenos Aires.

REFERENCES

1. For example, Gillan, M.J., *J. Chem. Soc., Faraday Trans. II*, 1989, **85**, 521; Mehl, M.J., Osburn, J.E., Papaconstantopoulos, D.A. and Klein, B.M., *Phys. Rev.*, 1990, **B41**, 10311.
2. Pisani, C., Dovesi, R. and Roetti, C., *Hartree–Fock Ab Initio Treatment of Crystalline Systems*, Springer-Verlag, Berlin, 1988.
3. Dovesi, R., Saunders, V.R. and Roetti, C., *CRYSTAL 92 User Documentation*, University of Torino and SERC Daresbury Laboratory, 1992.
4. For example, Ojamae, L., Hermansson, K., Dovesi, R., Roetti, C. and Saunders, V.R., *J. Chem. Phys.*, 1994, **100**, 2128; Catti, M., Pavese, A., Dovesi, R. and Saunders, V.R., *Phys. Rev.*, 1993, **B47**, 9189; Orlando, R., Azavant, P., Towler, M.D., Dovesi, R. and Roetti, C., *J. Phys. Condensed Matter*, 1996, **8**, 8573; Mackrodt, W.C., Harrison, N.M., Saunders, V.R., Allan, N.L. and Towler, M.D., *Chem. Phys. Lett.*, 1996, **250**, 66.
5. For a brief review, see Allan, N.L. and Mackrodt, W.C., *Phil. Mag.*, 1994, **B69**, 871.
6. Gale, J.D., Catlow, C.R.A. and Mackrodt, W.C., *Modelling Simul. Mater. Sci. Eng.*, 1992, **1**, 73.
7. Noda, K., Ishii, Y., Ohno, H., Watanabe, H. and Matsui, H., *Adv. Ceram.*, 1989, **25**, 155.
8. Tone, T., Fujisawa, N. and Seki, Y., *Nucl. Tech./Fus.*, 1983, **4**, 573.
9. Akiyama, M., Ando, K. and Oishi, Y., *Solid State Ionics*, 1981, **3–4**, 469.
10. Farley, T.W.D., Hayes, W., Hull, S., Ward, R., Hutchings, M.T. and Alba, M., *Solid State Ionics*, 1988, **28–30**, 189.
11. Chadwick, A.V., Flack, K.W., Strange, J.H. and Harding, J.H., *Solid State Ionics*, 1988, **28–30**, 185.
12. Strange, J.H., Rageb, S.M., Chadwick, A.V., Flack, K.W. and Harding, J.H., *J. Chem. Soc.,Farad. Trans.*, 1990, **86**, 1239; Flack, K.W., Ph.D thesis, University of Kent, 1990.
13. Farley, T.W.D., Hayes, W., Hull, S., Hutchings, M.T. and Vrtis, M., *J. Phys: Condens. Matter*, 1991, **3**, 4761.
14. Jacobs, P.W.M. and Vernon, M.L., *J. Chem. Soc., Farad. Trans*, 1993 **86**, 1233.
15. De Vita, M.L., Manassidis, Y., Lin, J.S. and Gillan, M.J., *Europhys. Lett.*, 1992, **19**, 605.
16. Gavartin, J.L., Catlow, C.R.A., Shluger, A.L., Varaksin, A.N. and Kolmogorov, Yu.N., *Modelling Simul. Mater. Sci. Eng.*, 1992, **1**, 29.
17. Gavartin, J.L., Catlow, C.R.A., Shluger, A.L., Jacobs, P.W.M. and Rycerz, Z.A., *Rad. Eff. Def. Sol.*, 1995, **133**.
18. Gavartin, J.L., Shluger, A.L. and Catlow, C.R.A., *J. Phys.: Condens. Matter*, 1993, **5**, 7397.
19. Dovesi, R., Roetti, C., Freyria-Fava, C., Prencipe, M. and Saunders, V.R., *Chem. Phys.*, 1991, **156**, 11.
20. McCarthy, M.I. and Harrison, N.M., *Phys. Rev.*, 1994, **B49**, 8574.
21. Allan, N.L., Mackrodt, W.C. and Rimmington, S., *Abstracts of the International Conference on Defects in Insulating Crystals*, University of Parma, August 1988, University of Parma, 1988; Mackrodt, W.C., *J. Mol. Liq.*, 1988, **39**, 121.
22. Bush, T.S., Gale, J.D., Catlow, C.R.A. and Battle, P.D., *J. Mat. Chem.*, 1994, **4**, 831.
23. Cooper, D.L., Thorsteinsson, T., Raimondi, M. and Gerratt, J., *Phil. Mag.*, 1996, **B73**, 175.
24. Chadi, D.J. and Cohen, M.L., *Phys. Rev.*, 1973, **B8**, 5747.
25. Venkataraman, G., Feldkemp, L.A. and Sahni, V.C., *Dynamics of Perfect Crystals*, MIT Press, Cambridge, 1975.
26. Melchionna, S., Ciccotti, G. and Hulian, B.L., *Molec. Phys.*, 1993, **78**, 533.
27. Kurasawa, T., Takahashi, T., Noda, K., Takeshita, H., Nasu, S. and Watanabe, H., *J. Nucl. Mat.*, 1982, **107**, 107.
28. Hull, S., Farley, T.W.D., Hayes, W. and Hutchings, M.T., *J. Nucl. Mat.*, 1988, **160**, 125.
29. Fincham, D., Mackrodt, W.C. and Mitchell, P.J., *J. Phys. C: Condens. Matter*, 1994, **6**, 393.
30. Roberts, R.B. and White, G.K., *J. Phys. C: Solid State Phys.*, 1986, **19**, 7167.
31. Liu, Y.Y., Billone, M.C., Fischer, A.K., Tan, S.W. and Clemmer, R.G., *J. Fus. Tech.*, 1985, **8**, 1970.
32. For example, Gillan, M.J. and Richardson, D.D., *J. Phys. C: Solid State Phys.*, 1979, **12**, L61; Walker, J.R. (ch. 5), Dixon, M. and Gillan, M.J. (ch. 18) in *Computer Simulation of Solids*, ed. C.R.A. Catlow and W.C. Mackrodt, Lecture Notes in Physics, Vol. 166, Springer-Verlag, Berlin, 1982.
33. Oishi, Y., Kamei, Y., Akiyama, M. and Yanagi, T., *J. Nucl. Mater.*, 1979, **87**, 341.
34. Akiyama, M., Ando, K. and Oishi, Y., *Solid State Ionics*, 1981, **3/4**, 469.
35. For example, Payne, M.C., Teter M.P., Allan, D.C., Arias, T.A. and Joannopoulos, J.D., *Rev. Mod. Phys*, 1992, **64**, 1045.